XN-NF-79-6(NP)

EXXON NUCLEAR ANALYSIS OF POWER DISTRIBUTION MEASUREMENT UNCERTAINTY FOR WESTINGHOUSE PWR'S

JULY 1979

RICHLAND, WA 99352

EXXON NUCLEAR COMPANY, Inc.

7908210569

758 290

XN-NF-79-6 (NP)
ISSUE DATE: 7/23/79

EXXON NUCLEAR ANALYSIS OF POWER DISTRIBUTION MEASUREMENT UNCERTAINTY FOR WESTINGHOUSE PWR'S

Prepared by: J. S. Holm

Contributors: H. W. Graves, Jr.
J. L. Jaech

Approved by: 6/22/79
R. B. Stout, Manager
Neutronics Development

6/22/79
F. B. Skogen, Manager
PWR Neutroncis

6/25/79
J. N. Morgan, Manager
Neutronics & Fuel Management

6-25-79
G. A. Sofer, Manager
Nuclear Fuels Engineering

6-26-79
G. F. Owsley, Manager
Reload Licensing

758 291

NUCLEAR REGULATORY COMMISSION DISCLAIMER

IMPORTANT NOTICE REGARDING CONTENTS AND USE OF THIS DOCUMENT

PLEASE READ CAREFULLY

This technical report was derived through research and development programs sponsored by Exxon Nuclear Company, Inc. It is being submitted by Exxon Nuclear to the USNRC as part of a technical contribution to facilitate safety analyses by licensees of the USNRC which utilize Exxon Nuclear-fabricated reload fuel or other technical services provided by Exxon Nuclear for light water power reactors and it is true and correct to the best of Exxon Nuclear's knowledge, information, and belief. The information contained herein may be used by the USNRC in its review of this report, and by licensees or applicants before the USNRC which are customers of Exxon Nuclear in their demonstration of compliance with the USNRC's regulations.

Without derogating from the foregoing, neither Exxon Nuclear nor any person acting on its behalf:

A. Makes any warranty, express or implied, with respect to the accuracy, completeness, or usefulness of the information contained in this document, or that the use of any information, apparatus, method, or process disclosed in this document will not infringe privately owned rights; or

B. Assumes any liabilities with respect to the use of, or for damages resulting from the use of, any information, apparatus, method, or process disclosed in this document.

TABLE OF CONTENTS

LIST OF TABLES

LIST OF FIGURES

758 295

1.0 INTRODUCTION

Full core measured power distributions must be periodically determined in nuclear reactors. The power distribution is determined through the use of measured and calculated data and thus necessarily contains a degree of uncertainty. This report presents an analysis of the uncertainty in the measured power distribution in Westinghouse PWR's using Exxon Nuclear Company methods.

Data for the analysis were obtained from three reactors: D. C. Cook, H. B. Robinson, and R. E. Ginna. One cycle of operating data, power distribution measurements, were utilized from each plant. Measured data for assembly local power distributions were obtained from critical experiments performed by Babcock & Wilcox and Battelle Pacific Northwest Laboratories.

Access of this report to individual utility reactor license application is through special permission by Exxon Nuclear Company, Inc.

2.0 SUMMARY

The analysis presented in this report evaluates the uncertainty associated with a three-dimensional and a two-dimensional measured power distribution. This uncertainty evaluation indicates that the one sided 95-95 tolerance limit associated with the three-dimensional power distribution is [ ]*. There is a 95% probability that the three-dimensional power distribution will not exceed [ ] times the measured value at a 95% confidence level. The corresponding value for the two-dimensional power distribution is [ ]. These results support the present Technical Specification values for measurement uncertainties of 5% for F_Q and 4% for $F_{\Delta H}$. F_Q is defined as the peak relative power density in the core. $F_{\Delta H}$ is the peak axially integrated pin power relative to the average axially integrated pin power. The three-dimensional measured power distribution uncertainty is applicable to F_Q and the two-dimensional measured power distribution uncertainty is applicable to $F_{\Delta H}$. A summary of the results of this report is presented in Table 2.1. The table depicts the final results and the components of the final result.

The incore instrumentation system used in Westinghouse PWR's consists of an array of detector thimbles which extend the full length of the core in approximately thirty percent of the fuel assemblies. The starting point for a power distribution measurement consists of a set of activation traces obtained from each of these thimbles using small moveable U-235 fission chambers. Since the instrumentation thimbles are distributed approximately uniformly throughout the core, those assemblies which do not contain thimbles are located closely to assemblies which do.

---

*Information proprietary to Exxon Nuclear Company, Inc. has been deleted and will be denoted in this fashion for the remainder of this report.

758 296

A calculated activation distribution and a calculated power distribution are used to extrapolate from the measured activation distribution to a "measured" power distribution for all assemblies in the core. A salient feature of the measurement procedure is the use of, in many cases, several nearby thimbles to determine the activation in unmeasured locations. This procedure not only reduces statistical uncertainties associated with the measurement process, but also tends to average out any errors associated with the calculated neutron flux distribution. Few group diffusion theory and transport theory calculations are then used to convert the axial activation distribution in each instrumented assembly to a full core power distribution. Section 3.0 of this report presents a detailed description of the computational procedure used to convert the measured activation distribution obtained from the instrumentation system to a three-dimensional "measured" power distribution.

The uncertaintites associated with the evaluation of the three-dimensional power distribution and the two-dimensional power distribution stem from three sources: the experimental uncertainties associated with the activation measurements, the computational uncertainty associated with extrapolating from the measured activation distribution in 30% of the assemblies to the "measured" power distribution in all assemblies (coupling factor uncertainty), and the computational uncertainty associated with calculating the assembly local power distribution. Section 4.0 presents a detailed evaluation of these uncertainty sources. This evaluation is based on measurements in three operating reactors, as well as measurements in several cold, clean critical experiments which have been used to confirm the detailed pin by pin power distribution computational procedure.

758 294

Table 2.1 Summary of Measurement Uncertainties

758 299

3.0 DETERMINATION OF THE MEASURED RELATIVE POWER DISTRIBUTION

The measured relative power distribution is determined by combining physically measured three-dimensional data with calculated two-dimensional data. The measured data consists of activation measurements with a detector containing U-235, in instrument thimbles located in approximately thirty percent of the assemblies in the core. The calculated data consists of two-dimensional power distributions and activation distributions determined using transport and diffusion theory codes.

ENC calculates the power and activation distribution using the codes PDQ(1)/HARMONY(2) with cross sections from XPOSE(3) and activation correction factors from the transport theory code XPIN(4). The ENC calculational methodology is discussed in detail in References 5, 6, and 7. The physically measured data and the calculated data are combined in codes such as INCORE(8) and DETECTOR(9) to yield the measured relative power distribution.

The measurement system used in Westinghouse reactors is described in Reference 10. Briefly the measurement system consists of instrument thimbles, detectors, a detector drive mechanism and a computer to record the electronic signal from the detectors. The instrument thimbles are located near the assembly center and consist of hollow tubes through which the detectors pass. The detectors are ionization chamber detectors using U-235 as the fissionable isotope. As the detector is driven through the instrument thimble at a constant rate of speed the incident neutrons causes the U-235 to fission. The fission products ionize a gas in the detector and produce an electric

758 300

current. The electronic signal is recorded as the detector moves through the instrument tube and provides an axially distributed measurement of the activation. The locations of the instrument tubes in typical 2, 3, and 4-loop plants are shown in Figures 3.1, 3.2, and 3.3.

3.1 DESCRIPTION OF THE DETERMINATION OF THE MEASURED RELATIVE POWER DISTRIBUTION

The measured relative power distribution is determined as the product of measured and calculated components. The basic equation is:

$$P^m(x,y,z) = \frac{\sum_{x',y'} W(x,y,x',y')\ P^c(x,y)\ L^c(x,y,)\quad A^m(x',y',z)/A^c(x',y')}{\text{average over } x,y,z \text{ of above terms (excluding } L^c(x,y)} \qquad (3.1)$$

where the terms are defined as:

$P^m(x,y,z)$:	Measured relative power distribution.
$W(x,y,x',y')$:	Weighting factor for position x',y' as used in determining power at x,y. $(\sum_{x',y'} W(x,y,x',y') = 1.0)$
$P^c(x,y)$:	Calculated relative assembly power.
$A^m(x',y',z)$:	Measured relative activation rate at axial position z in instrument thimble located at x',y'.
$A^c(x,y)$:	Calculated relative activation rate in instrument thimble located at x,y.
$L^c(x,y)$:	Calculated local assembly power factor.

The resultant relative power distribution is discrete since there are only a finite number of assemblies, and thus (x,y) positions, in the core and a finite number of axial points at which data are taken. The two-dimensional peak pin power distribution, $P^m(x,y)$, can be determined by integrating equation 3.1 over z. Table 3.1 defines various symbols used in this report including those in Equation 3.1.

The codes DETECTOR and INCORE implement Equation 3.1. This implementation will be briefly described. A more detailed understanding of these codes can be obtained from the References 9 and 8. The discussion to follow will be based upon the code DETECTOR. For the uncertainty analysis, Equation 3.1 provides sufficient information about the codes.

The measured activation distribution is input to the code in the form of axial data points accompanied by a background signal value, a detector identifier, and an amplifier scale setting. The code adjusts the measured data for background, amplifier setting, and normalizes the data from different detectors. The normalization is performed by measuring the activation in a single assembly with each of the detectors. Detector specific normalization factors are determined such that the integral response of each detector in the common assembly is identical. The measured data is multiplied by these normalization factors to produce a three-dimensional activation distribution.

Calculated power and activation distributions are input to the code as a function of exposure and control rod insertion. At hot full power conditions the control bank is normally slightly inserted into the core.

Calculated data are therefore supplied for an unrodded core condition and a fully inserted control bank condition. In Equation 3.1 the distribution corresponding to the fully rodded configuration is used for values of z which correspond to rodded planes and the unrodded distribution is used for unrodded planes.

The power at an unmeasured location (x,y) is determined from measurements at locations (x',y'). The measurements used to determine the power at (x,y) are those which are within a specified radius of (x,v). The value for the radius is input to the code.

3.2 COMPARISON OF INCORE AND DETECTOR RESULTS

The DETECTOR code was used for the analysis presented in this report. However, the results and conclusions in this report are applicable if the INCORE code is used instead of DETECTOR. To verify this a comparison of the two codes was made.

The codes DETECTOR and INCORE both use a similar mathematical formulation as described in Section 3.1. To demonstrate the similarity between the two codes, both were used to determine the measured power distribution for two power maps taken at the R. E. Ginna plant, Cycle 8, at 1,746 MWD/MT and 4,611 MWD/MT. The INCORE results are from the standard power distribution measurements taken at the plant. The DETECTOR calculations were performed by ENC using the plant measured data and ENC calculational data that were input to INCORE.

The measurement of $F_Q^N(z)$ and of the peak values for F_Q^N, $F_{\Delta H}^N$, and F_z are shown in Tables 3.2 and 3.3. As indicated by the comparisons shown in

758 303

the tables, the two codes yield nearly identical results. The differences between the peak values are less than 0.5%. The axial F_Q^N distribution is nearly identical except at the top and bottom points of the core. The differences here are due to the fact that DETECTOR smooths the data to remove the effects of measurements of the flux peak in the reflector regions and INCORE does not.

Comparisons of assembly power distributions from DETECTOR and INCORE for identical input are shown in Figures 3.4 and 3.5. The distributions are nearly identical with most differences less than a few tenths of a percent. These comparisons justify that the results of this report are equally applicable for either of the two codes.

Table 3.1 Definition of Symbols

$A^c(x,y)$:	Calculated two-dimensional relative activation distribution.
$A^m(x,y,z)$:	Measured three-dimensional relative activation distribution.
$A^m(x,y)$:	Measured two-dimensional relative activation distribution.
K:	One sided 95-95 tolerance limit factor.
KS_z:	One sided 95-95 tolerance limit for the variable denoted by z, i.e. KS_{P^m}/P^m, KSP^m_{xy}/P^m_{xy}.
$L^c(x,y)$:	Calculated assembly local power factor.
N_d:	Average number of instrument thimbles utilized in extrapolating from measured to nonmeasured location.
$P^c(x,y)$:	Calculated two-dimensional relative power distribution.
$P^m(x,y)$:	Measured two-dimensional relative power distribution.
$P^m(x,y,z)$:	Measured three-dimensional relative power distribution.
S_a/a:	Relative standard deviation for an axial point.
S_{A^m}/A^m:	Relative standard deviation for the measured three dimensional activation distribution.
$S_{A^m_{xy}}/A^m_{xy}$:	Relative standard deviation for the measured two-dimensional activation distribution.
S_{CF}/CF:	Relative standard deviation for the calculated coupling factor.
S_I/I:	Relative standard deviation for the integral of the measured axial activation distribution.
S_{L^c}/L^c:	Relative standard deviation for the local assembly power distribution.
S_{P^m}/P^m:	Relative standard deviation for the measured three-dimensional power distribution.
$S_{P^m_{xy}}/P^m_{xy}$:	Relative standard one deviation for the measured two-dimensional power distribution.
W(x,y;x',y'):	Weighting factor for extrapolating from location (x' , y') to location (x,y).

905

758

Table 3.2 Axial F_Q^N Distribution; Comparison Between INCORE and DETECTOR Results, R. E. Ginna, Cycle 8, 1,746 MWD/MT, Hot Full Power

	Axial F_Q^N			Axial F_Q^N	
Node	DETECTOR	INCORE	Node	DETECTOR	INCORE
Top 55	.669	.727	20	1.467	1.465
54	.717	.703	19	1.455	1.451
53	.886	.875	18	1.394	1.391
52	.972	.966	17	1.399	1.396
51	1.068	1.060	16	1.454	1.451
50	1.217	1.214	15	1.470	1.467
49	1.293	1.290	14	1.470	1.467
48	1.346	1.343	13	1.470	1.467
47	1.386	1.383	12	1.451	1.448
46	1.405	1.402	11	1.416	1.413
45	1.419	1.413	10	1.320	1.318
44	1.411	1.402	9	1.304	1.300
43	1.288	1.282	8	1.334	1.332
42	1.429	1.421	7	1.293	1.291
41	1.468	1.460	6	1.228	1.226
40	1.475	1.467	5	1.136	1.134
39	1.483	1.475	4	.995	.994
38	1.471	1.463	3	.819	.819
37	1.442	1.436	2	.563	.562
36	1.339	1.333	Bottom 1	.563	.760
35	1.458	1.451			
34	1.471	1.465			
33	1.475	1.469			
32	1.467	1.461			
31	1.433	1.429			
30	1.349	1.344			
29	1.462	1.457			
28	1.478	1.476			
27	1.472	1.470			
26	1.470	1.466			
25	1.432	1.429			
24	1.365	1.360			
23	1.457	1.455			
22	1.472	1.468			
21	1.474	1.470			

	DETECTOR	INCORE	% DIFFERENCE
F_Q^N	1.483	1.476	.47
$F_{\Delta H}^N$	1.305	1.302	.23
F_z	1.135	1.131	.35

Table 3.3 Axial F_Q^N Distribution; Comparison Between INCORE and DETECTOR Results, R. E. Ginna, Cycle 8, 4,611 MWD/MT, Hot Full Power

	Axial F_Q^N	
Node	DETECTOR	INCORE
Top 55	.676	.741
54	.730	.739
53	.884	.882
52	.942	.935
51	1.048	1.025
50	1.177	1.167
49	1.234	1.230
48	1.278	1.274
47	1.309	1.305
46	1.323	1.319
45	1.325	1.321
44	1.314	1.307
43	1.189	1.183
42	1.316	1.309
41	1.354	1.348
40	1.365	1.359
39	1.365	1.359
38	1.365	1.359
37	1.338	1.333
36	1.227	1.223
35	1.349	1.344
34	1.371	1.366
33	1.367	1.362
32	1.365	1.361
31	1.339	1.336
30	1.251	1.246
29	1.367	1.362
28	1.393	1.390
27	1.393	1.390
26	1.393	1.390
25	1.355	1.353
24	1.286	1.280
23	1.397	1.392
22	1.418	1.414
21	1.426	1.423
20	1.437	1.423
19	1.426	1.422
18	1.345	1.342
17	1.393	1.389
16	1.449	1.446
15	1.471	1.468
14	1.483	1.480
13	1.489	1.486
12	1.486	1.483
11	1.456	1.452
10	1.337	1.336
9	1.383	1.379
8	1.412	1.408
7	1.382	1.379
6	1.327	1.324
5	1.229	1.225
4	1.093	1.095
3	.891	.894
2	.665	.663
Bottom 1	.665	.877

	DETECTOR	INCORE	% DIFFERENCE
F_Q^N	1.489	1.486	.20
$F_{\Delta H}^N$	1.267	1.265	.16
F_z	1.164	1.162	.17

758 303

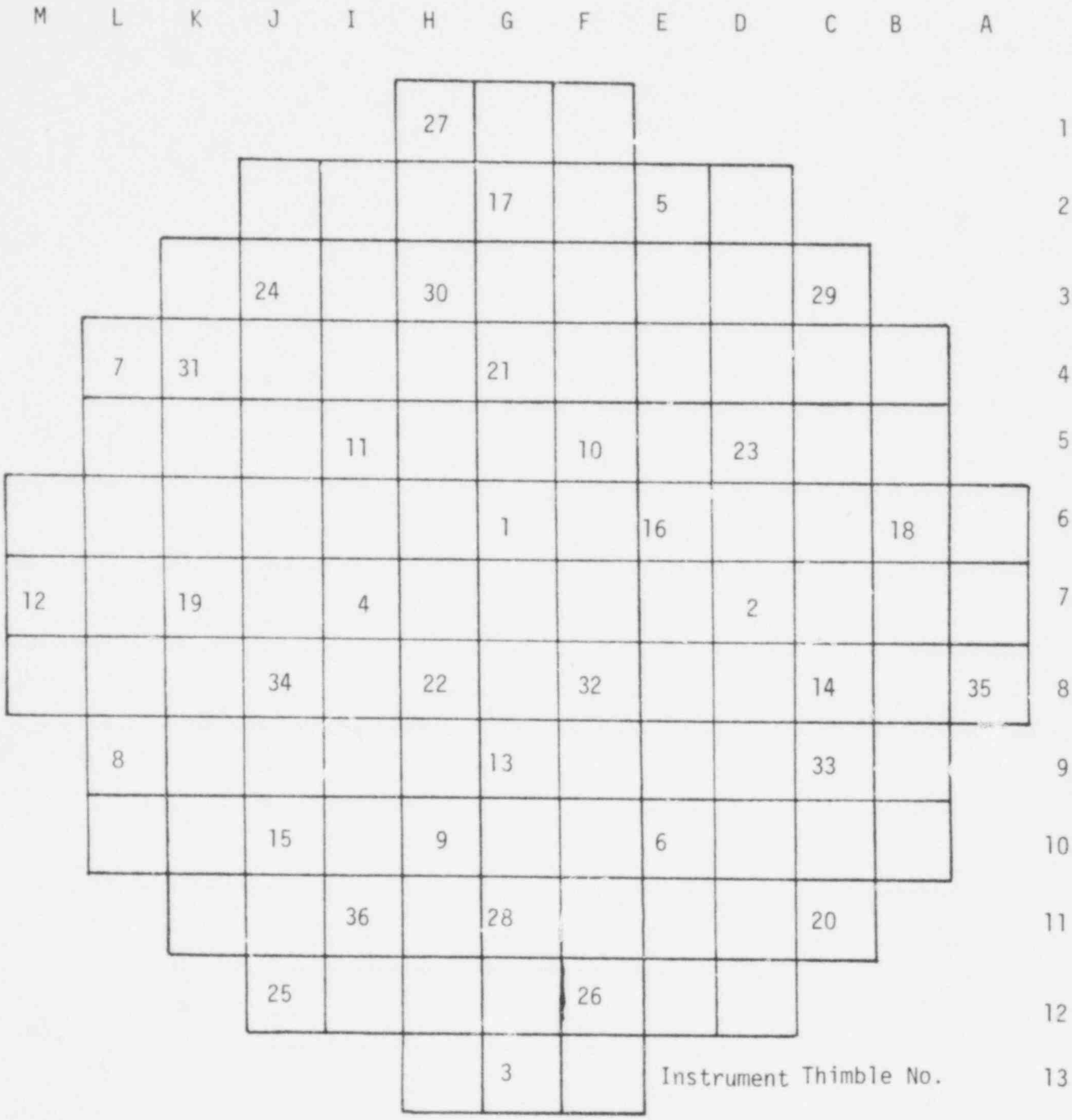

Figure 3.1 R. E. Ginna, Instrument Thimble Location, 2-Loop Core

758 308

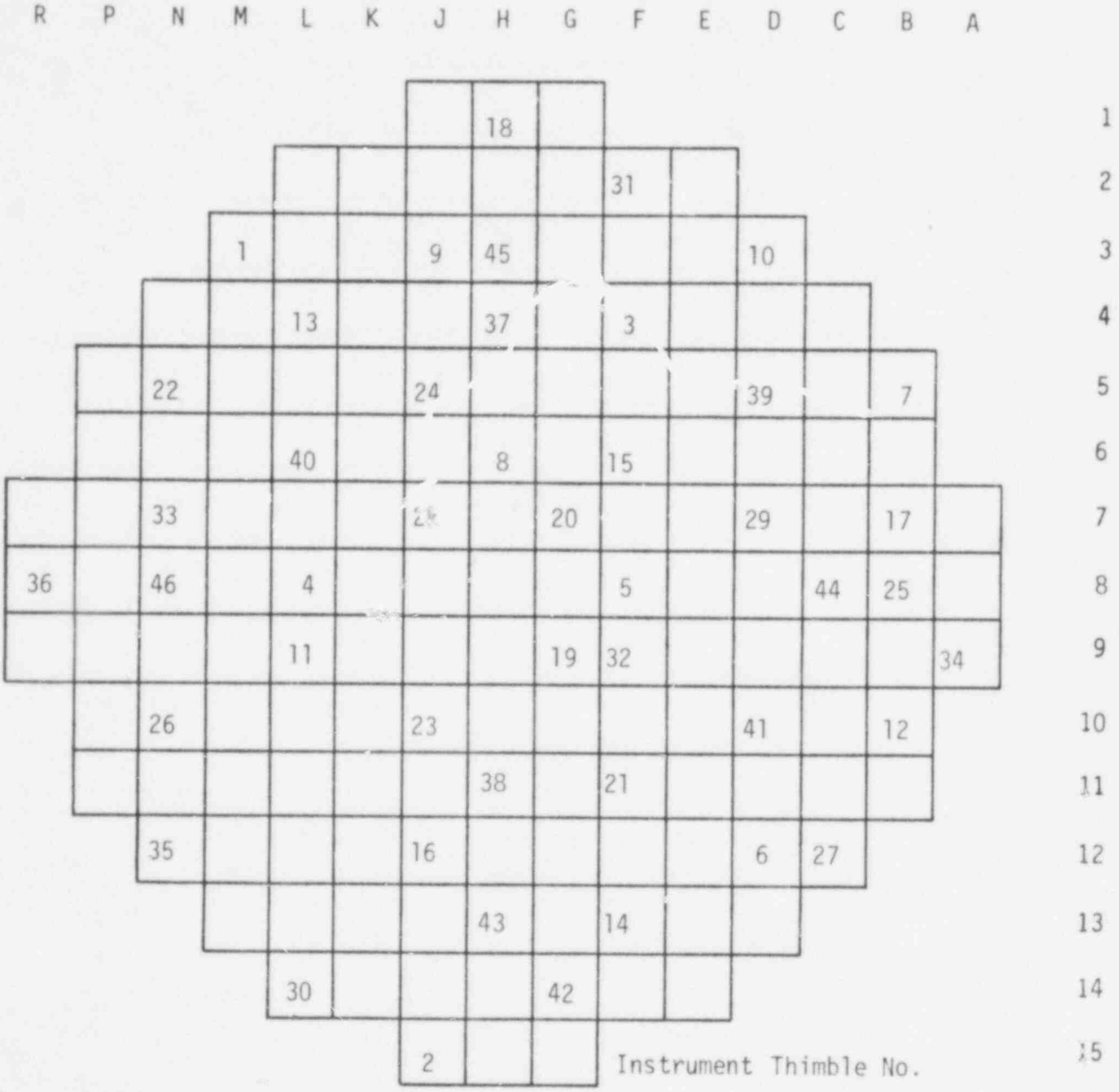

Figure 3.2 H. B. Robinson Instrument Thimble Locations, 3-loop Core

	R	P	N	M	L	K	J	H	G	F	E	D	C	B	A
1							28			15					
2			19			3		51							
3								10		30		39		52	
4		5	36					43							
5					11				38		31		24		
6	17		54			14		6						8	
7				44			32			16			47		
8	23		58		29		46			48		50	49	34	
9		57							22		9				56
10					4		1					12			
11	33				40			26			21				13
12						41			55			7			
13			45		35			20						25	
14			18				27			42		37			
15					53			2							

Instrument Thimble No.

Figure 3.3 D. C. Cook Unit 1, Instrument Thimble Locations, 4-Loop Core

758 310

	M	L	K	J	I	H	G	F	E	D	C	B	A
1						.673 .675	.824 .825	.668 .669					
2				.659 .659	.944 .945	1.134 1.135	1.051 1.051	1.134 1.136	.941 .944	.652 .662			
3			.734 .733	1.062 1.062	.989 .990	1.108 1.102	1.177 1.172	1.123 1.124	1.019 1.003	1.065 1.066	.731 .732		
4		.677 .682	1.065 1.059	1.038 1.036	1.195 1.200	1.046 1.045	.987 .989	1.053 1.054	1.195 1.195	1.031 1.031	1.064 1.065	.650 .653	
5		.969 .971	1.012 1.009	1.210 1.213	1.028 1.029	1.066 1.069	1.075 1.076	1.059 1.062	1.001 1.002	1.186 1.184	.996 .998	.939 .941	
6	.680 .682	1.146 1.150	1.118 1.125	1.064 1.066	1.078 1.079	.991 .991	1.149 1.149	.984 .985	1.062 1.064	1.052 1.054	1.125 1.124	1.133 1.135	.667 .669
7	.836 .837	1.060 1.063	1.184 1.182	.993 .994	1.089 1.090	1.164 1.167	1.030 1.030	1.165 1.167	1.082 1.082	.996 .997	1.191 1.187	1.060 1.059	.828 .829
8	.679 .680	1.147 1.150	1.131 1.132	1.055 1.054	1.073 1.074	1.005 1.011	1.167 1.167	1.002 1.004	1.072 1.074	1.046 1.047	1.129 1.126	1.154 1.153	.680 .680
9		.953 .955	1.010 1.009	1.201 1.200	1.010 1.010	1.068 1.069	1.089 1.086	1.067 1.068	1.001 .998	1.185 1.187	1.010 1.012	.957 .959	
10		.660 .662	1.076 1.078	1.049 1.049	1.200 1.200	1.052 1.052	.993 .992	1.045 1.044	1.178 1.177	1.037 1.036	1.082 1.083	.672 .672	
11			.747 .747	1.086 1.086	1.017 1.016	1.133 1.133	1.178 1.175	1.112 1.112	.989 .990	1.078 1.081	.748 .750		
12				.677 .679	.972 .971	1.150 1.151	1.051 1.051	1.123 1.119	.928 .930	.677 .678			
13						.677 .678	.828 .832	.668 .669	← INCORE ASSEMBLY POWER ← DETECTOR ASSEMBLY POWER				

Figure 3.4 Assembly Radial Power Distribution, Comparison of INCORE and DETECTOR Results, R. E. Ginna, Cycle 8, 1,746 MWD/MT Hot Full Power

758 311

	M	L	K	J	I	H	G	F	E	D	C	B	A
1						.686 .686	.837 .837	.695 .694					
2				.688 .688	.945 .949	1.115 1.115	1.044 1.047	1.126 1.125	.960 .958	.688 .689			
3			.754 .754	1.067 1.069	.995 .994	1.098 1.091	1.154 1.156	1.115 1.116	1.010 1.005	1.070 1.071	.757 .757		
4		.690 .694	1.060 1.054	1.033 1.031	1.182 1.184	1.047 1.045	.995 .998	1.052 1.054	1.180 1.181	1.032 1.033	1.069 1.070	.686 .687	
5		.960 .962	1.000 .998	1.188 1.190	1.024 1.025	1.072 1.073	1.082 1.082	1.065 1.066	1.004 1.004	1.176 1.175	1.002 1.003	.957 .958	
6	.691 .692	1.125 1.125	1.116 1.114	1.062 1.062	1.080 1.081	1.003 1.002	1.151 1.150	.996 .996	1.064 1.064	1.047 1.047	1.113 1.114	1.126 1.127	.694 .695
7	.839 .840	1.044 1.044	1.184 1.165	.999 .998	1.093 1.095	1.164 1.166	1.038 1.037	1.163 1.163	1.082 1.081	.994 .995	1.163 1.168	1.048 1.049	.839 .839
8	.690 .692	1.123 1.124	1.116 1.116	1.055 1.052	1.075 1.076	1.010 1.014	1.161 1.161	1.007 1.007	1.071 1.072	1.047 1.048	1.119 1.119	1.130 1.130	.691 .691
9		.952 .954	1.005 1.005	1.185 1.185	1.011 1.011	1.069 1.069	1.086 1.083	1.070 1.070	1.007 1.006	1.179 1.178	1.010 1.008	.962 .962	
10		.682 .683	1.071 1.074	1.041 1.043	1.181 1.181	1.048 1.048	.993 .992	1.047 1.047	1.175 1.177	1.035 1.035	1.075 1.075	.693 .693	
11			.764 .765	1.077 1.077	1.007 1.004	1.114 1.112	1.153 1.152	1.105 1.103	.998 1.000	1.073 1.075	.761 .763		
12				.694 .696	.966 .967	1.123 1.122	1.037 1.037	1.112 1.112	.946 .946	.692 .694			
13						.688 .689	.834 .836	.687 .687					

← INCORE ASSEMBLY POWER
← DETECTOR ASSEMBLY POWER

Figure 3.5 Assembly Radial Power Distribution, Comparison of INCORE and DETECTOR Results, R. E. Ginna, Cycle 8, 4,611 MWD/MT, Hot Full Power

758 312

4.0 UNCERTAINTY ANALYSIS FOR THE MEASURED RELATIVE POWER DISTRIBUTION

The analysis of the uncertainty for the measured relative power distribution begins with the equation for the determination of the measured relative power distribution. Deriving the measurement uncertainty from a mathematical description of the measured power distribution identifies the major sources of uncertainty and the manner in which they should be combined. The value for the uncertainty determined in this manner is a comprehensive one. The equation for the measured three-dimensional power distribution is shown below as Equation 4.1. The terms in the equation are defined in Section 3.0 and in Table 3.1.

$$P^m(x,y,z) = \frac{\underset{x',y'}{} W(x,y;x',y')\ P^c(x,y)\ L^C(x,y)\ \ A^m(x',y',z')/A^c(x',y')}{\text{average over } x,y,z \text{ of above terms (excluding } L^C(x,y))} \qquad (4.1)$$

To properly analyze the uncertainty in calculated parameters measured data are necessary. The uncertainty in the calculated activation term, $A^c(x,y)$, can be derived from comparison to the measured activation data,

758 313

$A^m(x,y)$. The uncertainty in the local power factor $L^c(x,y)$, can be determined by comparison to critical experiments in which the pin power distributions were measured. There are no measurements of the calculated two-dimensional power distribution, $P^c(x,y)$, and thus this term is difficult to assess.

The difficulties presented by the lack of measured data for $P^c(x,y)$ can be surmounted by manipulation of Equation 4.1. Let:

[ ]

This formulation is appropriate in view of the manner in which $A^c(x,y)$ is determined. The calculated activation distribution is primarily dependent upon the PDQ calculated power distribution. The activation distribution is determined from PDQ calculated instrument thimble fluxes plus transport theory correction factors. Substituting for $A^c(x,y)$ in Equation 4.1 and neglecting the normalization term in the denominator, yields.

[ ] (4.2)

Define two additional terms, CF(x,y,x',y') and R(x,y,x',y') as follows:

[(4.3)

(4.4)]

Equation 4.2 can now be written as follows:

[ ] (4.5)

[ ]

The relative standard deviation as derived from equation 4.5, assuming independence between the variables is:

[ ] (4.6)

where:

S_{P^m}/P^m: Relative standard devation in $P^m(x,y,z)$.

S_R/R: Relative standard deviation in $R(x,y,x',y')$.

S_{A^m}/A^m: Relative standard deviation in $A^m(x',y'z)$.

S_{APR}/APR: Relative standard deviation in $APR(x,y)$.

S_{L^c}/L^c: Relative standard deviation in $L^c(x,y)$.

N_d: Average number of measurement used to extrapolate to x,y.

The relative standard deivation in $CF(x,y;x',y')$ can be expressed as:

[ ] (4.7)

758 315

Solving equation 4.7 for S_R/R and substituting into equation 4.6 yields the following expression for S_{P^m}/P^m.

[ ] (4.8)

[ ]

[ ] (4.9)

Equation 4.9 contains only the relative standard deviations associated with terms for which measured data exists. Equation 4.9 is the final form for the relative standard S_{P^m}/P^m. The following sections will describe the analysis of each of the component terms of S_{P^m}/P^m.

The standard deviations will be presented on a relative basis. This will be accomplished through the use of a transformation of the parameter of interest. If x is the parameter for which a relative standard deviation is sought then the relative stadard deviation can be determined as follows:

Let $y = \ln x$

Then $\sigma_y^2 = (\partial \ln x/\partial x)^2 \sigma_x^2$

$\sigma_y^2 = \sigma_x^2/x^2$

Thus, σ_y represents the relative standard deviation in x.

4.1 COUPLING FACTOR

The relative standard deviation in the calculated coupling factors can be determined from comparisons of measured and calculated coupling factors. The coupling factor from an assembly at x',y' to one at x,y (Equation 4.3) is

[ ]

Let CF^m_{lm} be the measured coupling factor from an assembly at (x^m, y^m) and

CF^c_{lm} be the calculated coupling factor corresponding to CF^m_{lm}.

The relative standard deviation of the differences between calculation and measurement is:

$$S_{CF'}/CF' = \left[\frac{\sum_{l=1} \sum_{m=1} (\ln CF^c_{lm} - \ln CF^m_{lm})^2}{J_T} \right]^{1/2} \quad (4.10)$$

where:

L: The number of measured assemblies.

J_i: The number of assemblies within a distance r of assembly i which are used.

J_T: The total number of coupling factors $= \sum_l J_l$.

The uncertainty in $S_{CF'}/CF'$ includes the measurement uncertainty which must be removed in order to estimate S_{CF}/CF, the relative standard deviation in the calculated coupling factor.

The data utilized to estimate the coupling factor relative standard deviation are from three reactors. One cycle from each plant is utilized. The measurements are at full power and were taken at various exposure points during the cycle. In all cases the rods were nearly withdrawn from the core. The measured coupling factors were determined from the unrodded portion of the core and compared to calculated coupling factors for the unrodded condition. The rodded portion of the core was not utilized since the calculations in the rodded portion conservatively overpredict the radial power peaking due to the fact that the calculations for the rodded portion of the core represent full rod insertion while the measurements are for partial rod insertion. The calculations used are based on ENC's present calculational procedures as presented in References 5, 6, and 7.

The relative standard deviation of the differences between the calculated and measured coupling factors for measurements from all three reactors are shown in Table 4.1. The table includes approximately an equal amount of data from each plant. The relative standard deviation is tabulated as a function of radius. That is, for a particular radius the measured and calculated coupling factors were determined for all instrumented assemblies within that radius of each other. The table also indicates the average number of measured coupling factors for each plant at a particular value of the radius in assembly pitches.

[ ]

The relative standard deviation of the coupling factor for a radius of [ ] assembly pitches is shown in Table 4.2 along with the number of data points used to determine the relative standard deviation for each map and the average number of instrumented locations used to extrapolate to nonmeasured locations.

758 318

The overall relative standard deviation in the coupling factor is [ ]. This value contains the measurement uncertainty which must be removed in order to determine the relative deviation in the calculated coupling factor. A total of 505 measurements were taken to estimate this number.

The average number of measurements used in extrapolating from a measured location to a nonmeasured location is shown in Table 4.2. The average number for the measurements shown is [ ]. The value should be similar for the three types of plants since the ratio of the number of assemblies with instrument thimbles to the number of assemblies in the core is nearly the same for each plant type; .298, .293, and .301 for the 2, 3, and 4 loop plants. The variation in the average number of measurements used in extrapolating varies from map to map because measurements are not taken in all possible locations each time. Application of the uncertainty associated with the extrapolated assemblies to all assemblies is conservative since approximately thirty percent of the assemblies are measured directly and do not use the coupling factors.

The method of combining the individual components of S_pm/P^m assumes that each component is independently and normally distributed. The coupling factor can be seen to be independent from the other components due to the fact that it is not involved in the determination of the other components of P^m. When a random variable, in this case the difference between measured and calculated coupling factors, represents the total effect of a number of independent factors, the distribution of that variable tends to be normal. The factors are often not identified, or even identifiable, and only the net effect of these factors is observed. The coupling factor is a calculated parameter and thus varies from "truth" as a function of the various parameters which determine its value; exposure, enrichment, cross section, diffusion theory approximations, etc. The combined effect of the parameters determining the calculated coupling factor is to produce differences between calculation and measurement which are normally distributed. As a function of a single parameter the differences may not be normally distributed with a mean and a standard deviation identical to that of the data as a whole.

Analysis of the available data discloses that there are subsets of the data whose means and standard deviations differ from one another. This can be observed if the data are grouped on the basis of reactors or fuel regions. When viewed as a single population, the data are adequately described by the normal distribution. The resulting normal distribution is made up of a number of subpopulations with different means; the effect of these subpopulations is to increase the variability in the observed data. Thus, treating the data as from a single population does not invalidate the analysis; the effect is reflected in the data.

The coupling factor differences above were subjected to a χ^2 test for normality. The results of these tests are shown in Tables 4.3, 4.4, and 4.5. A separate test was performed for each plant. The results indicate that the individual reactor populations from which the data were drawn may reasonably be represented by normal distributions. This is evidenced by the fact that the probability of a greater χ^2 value occurring due to chance alone is [ ] for D. C. Cook, [ ] for R. E. Ginna, and [ ] for H. B. Robinson. These probabilities are above any reasonable level of significance.

4.2 REPRODUCIBILITY

The relative standard deviation in the measured activation distribution can be estimated from repeated measurements. The repeatability data can be divided into two parts:

[ ]

The activation distribution is defined as follows:

$$A(x,y,z) = (I_k/I_o)\, a^k\, (x,y,z) \tag{4.11}$$

where:

I_k: The integral of the signal from detector k in the normalization thimble.

I_o: The integral of the signal from the normalization detector in the normalization thimble.

$a^k(x,y,z)$ The signal from detector k in the thimble located at x,y and axial position z, normalized to a single power level during the measurements.

The data used to estimate the relative standard deviation in the measurement of the activation distribution consists of repeated measurements of the activation in a thimble by a single detector. The term I_k/I_o therefore drops out of these data and must be reinserted to arrive at the relative standard deviation in $A^m(x,y,z)$.

The relative standard deviation of the value of an axial point, can be determined as follows:

[ ]

and

[ ] (4.12)

Then

[ ] (4.13)

where

N: Denotes the number of axial points.

J: Denotes the number of measurements.

I: Denotes an index over the measurements.

S_a/a: Denotes the relative uncertainty of a single axial point.

The axial points in those portions of the core where the axial flux varies rapidly are excluded from Equation 4.13. This is because difficulties in axially positioning the detectors in the thimbles from measurement to measurement causes the comparisons to be between different axial points. In regions where the flux varies slowly this adds only a small amount to the apparent variation between measurements. In regions where the flux varies rapidly the apparent variation can be quite large, as is the case near grids. This is a variation in the position of the detector not in the value of the measured activation, these points are therefore excluded from the determination of S_a/a.

The relative standard deviation in the integral of the instrument thimble activation measurements, all axial points included, can be determined as follows:

Let

$$I = \sum_{i=1}^{N} a_i$$

Then

$$S_I/I = \left(\frac{\sum_{i=1}^{M} (I_i - \bar{I})^2}{M-1} \right)^{1/2} \qquad (4.14)$$

where

$\bar{I}$ Average of the integrals in the thimble.

I_i The value of a single integral.

S_I/I Relative standard deviation in the integral.

M Number of integral measurements.

The data used to determine S_a/a are summarized in Table 4.6 The value for S_a/a is [ ] using [ ] data points. The data used to determine S_I/I are depicted in Figure 4.1 as a frequency plot. The value of S_I/I is [ ] with [ ] data points used. A χ^2 test for normality is shown in Table 4.7 for the integral data used to determine S_I/I. The population from which the data is drawn is not normal; it deviates from normality in that too many of the data points lie within $\pm$.1%. The standard deviation of [ ] is caused by a few outlying data points that are not representative of the bulk of the data. The outlying data points cannot be excluded since there is no reason to believe that they are atypical. The overall estimate of the standard deviation, [ ], is reasonably descriptive of the combined effects of most of the data having a smaller uncertainty plus these relatively few data points with larger uncertainty. In what follows the lack of normality will be neglected; this can be done because the error component is so small relative to the other errors affecting the measured relative power distributions.

The relative standard deviation for $A^m(x,y,z)$ consists of three terms: [ ]

Since two measurements are used to calculate this term it is twice that of a single measurement. The standard deviation for $A^m(x,y,z)$ is thus:

[ ] (4.15)

The relative standard deviation in the measurement of the radial activation distribution consists only of terms 2 and 3 and is thus:

[ ] (4.16)

Substituting into the above equation for S_a/a and S_I/I yields:

[ ]

4.3 LOCAL POWER DISTRIBUTION

The uncertainty in the assembly local peaking factor is determined by comparing calculated and measured data. The measured data are taken from References 11, 12, 13, and 14. These measurements were performed by Babcock & Wilcox, and Battelle Pacific Northwest Laboratories. The measurements are described in detail in the References.

Briefly, the measured data consists of pin power distribution data for one-eighth of a simulated 15x15 PWR assembly. The experiments were performed with cold, clean cores. Table 4.8 summarizes the local power distribution measurements.

The Battelle experiment consists of one simulated 15x15 assembly surrounded by a driver region. Measurements were made in both the simulated assembly and in the driver region. The fuel was enriched to 2.35 w/o U-235 with a fuel diameter of .44 inches and a fuel pin clad outer diameter of .5 inches. The lattice pitch was .75 inches. The simulated assembly had nine water holes.

The Babcock & Wilcox experiments consisted of two varieties. The first consisted of four test 15x15 assemblies each surrounded by a cannister and the cannister surrounded by a buffer zone and a driver region. The four test assemblies had seventeen water holes. The second variety consisted of nine simulated assemblies surrounded by a driver region. The simulated assemblies had one instrument tube and sixteen water holes. Both types of experiments used fuel enriched to 2.46 w/o in U-235, a fuel diameter of .405

758 325

inches and a pin clad outer diameter of .475 inches. The lattice pitch was .644 inches. All measurements were performed in the central assemblies.

The relative standard deviation can be expressed as:

$$S_L/L = \left(\frac{\sum_{x,y} (\ln LP^c(x,y) - \ln (LP^m(x,y))^2}{N} \right)^{1/2} \qquad (4.17)$$

where:

$LP^c(x,y)$: Calculated pin power distribution, normalized to an average value of 1.0.

$LP^m(x,y)$: Measured pin power distribution, normalized to an average value of 1.0.

N: Total number of pins in measurement.

As written above the term S_L/L includes the measurement uncertainty in $LP^m(x,y)$. This measurement uncertainty must be removed to determine S_Lc/L^c.

Table 4.9 summarizes the relative standard deviation results for the local power distribution. The table contains estimates from each critical experiment for S_L/L, S_Lc/L^c, the critical experimental measurement uncertainty, and the number of pins. The overall value for S_Lc/L^c from the data in Table 4.9 is [ ] using [ ] data points. Figures 4.2 through 4.7 depict the pin by pin differences between measurement and calculation for the critical experiments.

.758 326

A χ^2 test of normality for the local power distribution difference data is presented in Table 4.10. The probability of a greater χ^2 value is [ ]; there is no strong evidence to suggest that the population from which the data were drawn is not normal.

4.4 TOLERANCE LIMITS FOR THE MEASURED RELATIVE POWER DISTRIBUTION

The relative standard deviation for the measured relative power distribution is expressed in Equation 4.9. The equation is shown below:

[ ] (4.18)

The one sided 95-95 tolerance limit can be determined from the relative standard deviation by multiplying by K, the one sided 95-95 tolerance factor. S_{CF}/CF can be expressed in terms of $S_{CF'}/CF'$ and $S_{A^m_{xy}}/A^m_{xy}$ as follows:

[ ]

Twice the radial measurement uncertainty must be removed since two measured activation rates are used to determine the measured coupling factor.

Substituting into Equation 4.18 the values for S_{CF}/CF, S_{A^m}/A^m, S_{L^c}/L^c, and N_d of [ ] and [ ], respectively; yields, S_{P^m}/P^m = [ ]. The equation for $S_{P^m_{xy}}/P^m_{xy}$ is the same as for S_{P^m}/P^m except that $S_{A^m_{xy}}/A^m_{xy}$ is substituted for S_{A^m}/A^m. The resulting relative standard deviation is $S_{P^m_{xy}}/P^m_{xy}$ = [ ].

The one sided 95-95 tolerance factor is tabulated[15] as a function of the number of degrees of freedom associated with the relative standard deviation. The degrees of freedom can be calculated from Satterthwaite's[16] formula which is given below:

For a variance defined as:

$$S_0^2 = a_1 S_1^2 + a_2 S_2^2 + \dots + a_k S_k^2$$

The degrees of freedom are given by:

$$df_0 = 2\ S_o^4 \quad (a_1^2 S_1^4/df_1 + a_2^2 S_2^4/df_2 + \dots + a_k^2 S_k^4/df_k)$$

The degrees of freedom associated with S_{P^m}/P^m and $S_{P^m_{xy}}/P^m_{xy}$ can be determined from those associated with S_{CF}/CF, S_{A^m}/A^m, $S_{A^m_{xy}}/A^m_{xy}$, and S_{L^c}/L^c. The relative standard deviations and degrees of freedom are summarized in Table 4.11. The k factor[14] for S_{P^m}/P^m and $S_{P^m_{xy}}/P^m_{xy}$ is [ ] degrees of freedom, respectively.

158 328

The one sided 95-95 tolerance limits are determined by multiplying the relative standard deviation by its associated one sided 95-95 tolerance limit factor. The one sided 95-95 tolerance limit for the three-dimensional power distribution is denoted $KS_p m/P^m$ while that for the two-dimensional power distribution is $KS_{p_{xy}} m / P^m_{xy}$. Multiplying the relative standard deviation, $S_p m/P^m$ and $S_{p_{xy}} m / P^m_{xy}$ by their one sided 95-95 tolerance limit factor of [ ] results in; $KS_p m/P^m =$ and $KS_{p_{xy}} m / P^m_{xy} =$. This is the final result of the uncertainty analysis for the measured relative power distribution.

758 329

Table 4.1 Coupling Factor Relative Standard Deviation As a Function of Radius (Assembly Pitches)

758 330

Table 4.2 Coupling Factor Relative Standard Deviations For a Radius of [ ]Assembly Pitches

Table 4.3 χ^2 Test of Normality, D. C. Cook Coupling Factor Data [ ]

Table 4.4 χ^2 Test of Normality, R. E. Ginna Coupling Factor Data [ ]

[ ]

Table 4.5 χ^2 Test of Normality, H. B. Robinson Coupling Factor Data [ ]

[ ]

758 330

Table 4.6 Reproducibility: Relative Standard Deviation of an Axial Point

Table 4.7 χ^2 Test of Normality, Reproducibility, Axial Activation Integrals

[ ]

Table 4.8 Local Power Distribution Measurements

Measurement ID	Ref. No.	Core Diameter Inches	Lattice Pitch Inches	U-235 Enrich. w/o	No. Water Holes&Inst. Holes	Boron Concen. ppm
BAW Core VI-A Loading 7	14	52.2	.644	2.46	17	1,333
BAW Core VI-A Loading 5	14	52.2	.644	2.46	17	1,340
BPNL Loading GP-L99	11	29.3	.75	2.35	9	552
BAW Core XII Loading 1	13	52.2	.644	2.46	17	1,326
BAW Core XI Loading 2	12	52.2	.644	2.46	17	1,334
BAW Core XI Loading 3	12	52.2	.644	2.46	17	1,337

Table 4.9 Relative Standard Deviation for the Local Power Distribution

[ ]

Table 4.10 χ^2 Test of Normality, Local Power Distribution Data

[ ]

758 339

Table 4.11 Summary of Relative Standard Deviations and Associated Degress of Freedom

Figure 4.1 Reproducibility of the Integral of an Axial Activation Measurement

Figures 4.2 Local Power Distribution, BAW
Core VI-A Loading 7

Figure 4.3 Local Power Distribution, BAW Core VI-A Loading 5

Figure 4.4 Local Power Distribution BPNL Loading GP-L99

Figure 4.5 Local Power Distribution, BAW
Core XII Loading 1

Figures 4.6 Local Power Distribution, BAW
Core XI Loading 2

Figure 4.7 Local Power Distribution, BAW
Core IX Loading 3

758 348

5.0 REFERENCES

1. W. R. Caldwell, "PDQ7 Reference Manual", WAPD-TM-678, Westinghouse Electric Corporation, January 1967.

2. R. J. Breen, et al., "HARMONY: System for Nuclear Reactor Depletion Computation", WAPD-TM-478, Westinghouse Electric Corporation, January, 1965.

3. F. B. Skogen, "XPOSE - The Exxon Nuclear Revised LEOPARD", XN-CC-21, Revision 2, ENC April, 1975.

4. W. W. Porath, et al., "XPIN - The Exxon Nuclear Revised HAMBUR, Users Manual", XN-CC-26, Revision 1, ENC December 1975.

5. F. B. Skogen, "Exxon Nuclear Neutronic Design Methods for Pressurized Water Reactors", XN-75-27, ENC June, 1975.

6. F. B. Skogen, "Exxon Nuclear Neutronic Design Methods for Pressurized Water Reactors", XN-75-27, Supplement 1, ENC September, 1976.

7. F. B. Skogen, "Exxon Nuclear Neutronic Design Methods for Pressurized Water Reactors", XN-75-27, Supplement 2, ENC December, 1977.

8. W. D. Leggett, III and L. D. Eisenhart, "The INCORE Code", WCAP-7149, Westinghouse Electric Corporation, December, 1967.

9. S. C. Cohen, Phillip Hsiang and R. T. Shanstrom, "CORE: Codes for Operating Reactor Evaluation", Shanstrom Nuclear Associates, March 7, 1977.

10. "Evaluation of Nuclear Hot Channel Factor Uncertainties", WCAP-7810, December, 1971.

11. R. I. Smith, and L. D. Williams, "Measurements for Prototypical Plutonium Recycle Cores in Pressurized Water Reactors", Battelle Pacific Northwest Laboratories, March, 1973.

12. M. N. Baldwin, and M. E. Stern, "Physics Verification Program Part III Task 4", BAW-3647-20, Babcock & Wilcox, March, 1971.

13. M. N. Baldwin, and G. T. Fairburn, "Physics Verification Program Part III Tasks 5, 6, and 7", BAW-3647-24, Babcock & Wilcox, March, 1972.

548

14. R. H. Clark, M. N. Baldwin, W. G. Pettus, and T. G. Pitts, "Physics Verification Program Final Report", BAW-3647-3, Babcock and Wilcox, March, 1967.

15. D. B. Owen, "Factors for One-Sided Tolerance Limits and for Variable Sampling Plans", Sandia Corporation Monograph, SCR-607, March, 1963.

16. F. E. Satterthwaite, "An Approximate Distribution of Estimates of Variance Components", Biometrics Bull. 2 (1946), 110-114.

EXXON NUCLEAR ANALYSIS OF
POWER DISTRIBUTION MEASUREMENT
UNCERTAINTY FOR WESTINGHOUSE PWR'S

DISTRIBUTION LIST

J. S. Holm (2)

R. B. Stout

J. N. Morgan

G. A. Sofer

W. S. Nechodom

G. F. Owsley/NRC (21)

Document Control (10)

758 358